Carpe Momentum: Computing Kurtosis with Anomalous Diffusion Measures

Carson Ingo[1], Yu Fen Chen[2], Todd B. Parrish[2], Andrew G. Webb[1], and Itamar Ronen[1]

[1]*C.J. Gorter Center for High Field MRI, Department of Radiology, Leiden University Medical Center, Leiden, Netherlands,* [2]*Department of Radiology, Northwestern University, Chicago, IL, United States*

Target Audience Those interested in the characterization of neural tissue microstructure using new models for the non-Gaussian diffusion signal.

Purpose Excess kurtosis, K, is defined as the normalized fourth moment of a probability distribution function (pdf) with respect to the Gaussian pdf (i.e., K=3), as shown in Eq. (1). The first approach to estimate the apparent excess kurtosis, K_{app}, in non-Gaussian diffusion MRI used a Taylor series expansion approach to measure the deviation against the Gaussian case of a monoexponential decay, as shown in Eq. (2)[1]. Due to the parabolic form of the argument in Eq. (2), a limit must be placed on the maximum b-value sampled for the fitting function to monotonically decrease with increased diffusion weighting[2]. As very high strength (300 mT/m) gradients have recently become available for diffusion imaging, Eq. (2) becomes the barrier to interrogate tissue microstructure at high b-values[3]. Here, we present a new way to interpret and estimate kurtosis as anomalous subdiffusion, without restrictions on the maximum b-value.

Methods In anomalous diffusion theory, the mean squared displacement (MSD) is described by Eq. (3) where D is the diffusion coefficient, Γ is the generalized form of the factorial function defined for real numbers, and α is the power law parameter which describes the rate of subdiffusive growth when α<1. Note that when α=1 in Eq. (3) the MSD simply reduces to $2Dt$ to describe the linear case of Gaussian diffusion. In q-space, the diffusion MRI signal attenuation can be modeled by Eq. (4), where $t \equiv \Delta - \delta/3$ and E_α is the Mittag-Leffler function (MLF), which is an analytic and monotonically decreasing function for all arguments[4,5]. Eq. (4) can be expanded as a Taylor series to compute higher moments as shown in Eqs. (3) & (5) and by insertion into Eq. (1), the excess kurtosis of the MLF, K_{MLF}, is defined in Eq. (6). When α=1, for example, the MLF reduces to a monoexponential decay and K_{MLF}=0, pertaining to Gaussian diffusion. Eq. (6) is plotted in Fig. 1, which shows a nearly inverse linear relationship between K_{MLF} and α. Therefore, the monotonicity of the MLF provides an explicit means to interrogate the kurtosis of the pdf for the diffusion propagator without analytic limitations on q or Δ.

$$K \equiv \langle x^4 \rangle / \langle x^2 \rangle^2 - 3 \quad (1) \qquad S/S0 = exp\left(-bD + b^2 D^2 K_{app}/6\right) \quad (2)$$

$$\langle x^2(t) \rangle = 2Dt^\alpha / \Gamma(\alpha + 1) \quad (3) \qquad S/S0 = E_\alpha(-Dq^2 t^\alpha) \quad (4)$$

$$\langle x^4(t) \rangle = 24D^2 t^{2\alpha} / \Gamma(2\alpha + 1) \quad (5) \qquad K_{MLF} \equiv 6\,\Gamma^2(\alpha + 1)/\Gamma(2\alpha + 1) - 3 \quad (6)$$

To compare the estimates of kurtosis as computed by K_{app} and K_{MLF}, one chronic, ischemic stroke subject was scanned on a 3T Siemens Trio system. DW SE-EPI experiments were performed with the following parameters: TE=102 ms, TR=6 s, Δ=41.2 ms, δ=40.6 ms, b-values = 0, 500, 1000, 3000, 4000 s/mm^2, 3 diffusion weighted directions, NA=6, in-plane resolution = 2x2 mm, slice thickness=4 mm, 20 slices, scan time~6 min. The data were Rician noise corrected using an estimate of the signal variance in the right ventricle and then co-registered to the b=0 s/mm^2 image using SPM8. Using the Levenberg-Marquardt algorithm in Matlab, the trace of the 3 diffusion weighted direction data was fitted on a voxel-wise basis to Eqs. (1) and (3). The b=4000 s/mm^2 data was excluded for the fits to Eq. (1) to ensure a valid sample regime for the parabolic form[2]. Following estimations of α, the kurtosis, K_{MLF}, was computed using Eq. (5).

Results In Table 1, the values for D estimated from Eq. (2) are similar to D from Eq. (4). For completeness, D from Eq. (4) is shown in Fig. 2, however little contrast is visible between the WM and GM. In Fig. 2, for the α map, the contrast between the WM/GM is clearly visible with the WM demonstrating more subdiffusive behavior compared to the GM. The K_{MLF} map also has clearly visible WM/GM contrast and appears as a negative image to the α map. The K_{app} map has similar WM/GM contrast to K_{MLF}, albeit with a smaller dynamic range of values between the tissue types, as summarized for the regions of interest (ROI) comparisons in Table 1.

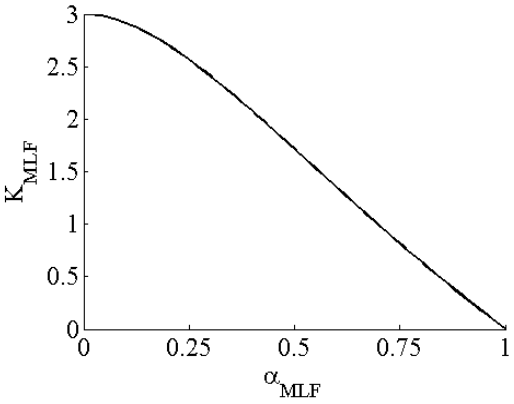

Fig. 1: Plot of Eq. (6) showing K_{MLF} versus α.

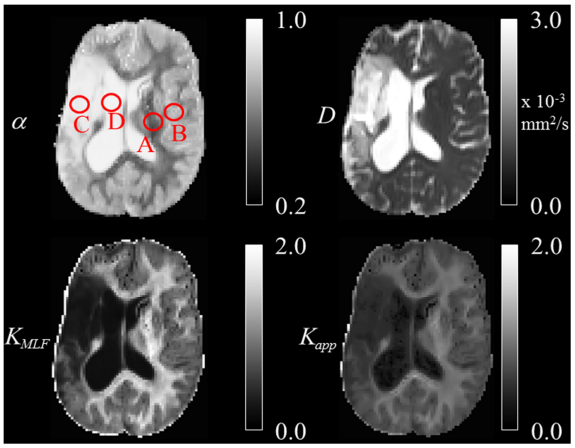

Fig. 2: Parameter maps for an axial slice through the brain of a chronic ischemic stroke patient with ROIs in the A) white matter (WM), B) gray matter (GM), C) ischemic tissue (IT), and D) cerebral spinal fluid (CSF).

Table 1: ROI mean and standard deviation values for D (reported in units of x10^{-3} mm^2/s), α, K_{MLF}, and K_{app}.

	WM	GM	IT	CSF
D (Eq. 2)	0.76 ± 0.04	0.82 ± 0.06	3.25 ± 0.11	3.31 ± 0.15
D (Eq. 4)	0.74 ± 0.03	0.86 ± 0.05	3.01 ± 0.11	3.15 ± 0.13
α	0.49 ± 0.04	0.77 ± 0.03	0.94 ± 0.03	0.97 ± 0.01
K_{MLF}	1.75 ± 0.12	0.75 ± 0.09	0.18 ± 0.09	0.12 ± 0.03
K_{app}	0.99 ± 0.07	0.58 ± 0.05	0.25 ± 0.03	0.19 ± 0.10

Discussion Utilizing the moment expansion in Eqs. (3) and (5) provides an intimate link between kurtosis to subdiffusion through the Γ function and α. However, this link does mean that Eq. (1) and Eq. (4) are interchangeable fitting functions, as each mathematical approach is a means to estimate the true kurtosis of the pdf. In Table 1, if we compare the estimated values for K_{MLF} and K_{app} in the ROIs, there is a consistent trend in which the WM exhibits higher kurtosis than the GM, and the IT and CSF have the lowest values. However, K_{MLF} estimates a wider dynamic range of kurtosis values for the ROIs compared to K_{app} such that the ratio for the mean values of WM to GM is ~2.27 for K_{MLF} and ~1.71 for K_{app}. One possible reason for the difference between K_{MLF} and K_{app} could be explained by considering that α operates on both the second and the fourth moments in Eqs. (3) and (5), whereas, in contrast, Eq. (2) defines the second moment as $2Dt$ and then carries the multiplicative factor into the fourth moment. Nevertheless, over a limited range of b-values, Eqs. (1) and (4) can produce similar, but not identical, estimations of kurtosis. As Eq. (4) is not bounded by a maximum b-value, the MLF provides the opportunity to more completely sample q-space to estimate the true kurtosis of the diffusion propagator, so long as there is sufficient signal-to-noise.

Conclusion We have shown a model for anomalous diffusion can provide an alternate, yet congruent approach to Eq. (1) to perform diffusion kurtosis imaging measurements. Current work is underway to apply Eq. (6) to extract physical properties of tissue microstructure (e.g. surface to volume ratio). Future work will characterize the directional dependence of estimations for α and K_{MLF} with respect to K_{app} in tensor representations.

References [1] Jensen JH, et al. Magn Reson Med 2005 1432-1440. [2] Jensen JH and Helpern JA. NMR Biomed 2010 698-710. [3] McNab JA, et al. Neuroimage 2013 234-245. [4] Metzler R and Klafter J. Phys Rep 2000 1-77. [5] Ingo C, et al. Magn Reson Med 2014 617-627.